Optics for high-efficiency full spectrum photovoltaics

Thesis by
Sunita Darbe

In Partial Fulfillment of the Requirements for the
degree of
Ph.D in Materials Science

CALIFORNIA INSTITUTE OF TECHNOLOGY
Pasadena, California

2017
(Defended October 24, 2016)

Sunita Darbe
ORCID: 0000-0002-8099-1814

ACKNOWLEDGEMENTS

There were many people who enabled this work in a variety of ways. First, thanks to my advisor Professor Harry Atwater who ambitiously started the Full Spectrum photovoltaics project and invited me to participate in it. He provided on-going optimism, an endless supply of ideas, and the resources to tackle the wide range of tasks this project would require. My work was funded by the Advanced Research Projects Agency-Energy (ARPA-E), U.S. Department of Energy, under Open 2012 Award Number DE-AR0000333 and MOSAIC Program Award ARPA-E Award No. DE-AR0000627 and the Dow Chemical Company through its University Partnership Program.

The Full Spectrum Photovoltaics project was carried out by a large team that provided support throughout my graduate career. Emily Kosten was an example of skepticism and showed me the value of not accepting something until I have convinced myself why. Emily Warmann was a consistent collaborator throughout prototyping and simulation efforts – making CPC, CAD designs and mechanical parts. Her optimization of bandgaps for spectrum splitting photovoltaics and work on annual energy production also provided a crucial basis for much of our system design efforts. Matthew Escarra was a mentor to me throughout my graduate career, collaborating closely on the holographic spectrum splitting work. My work on cost modeling was a small addition to primary work done by Kelsey Whitesell-Horowitz. Carissa Eisler was my conference roomie, confidant and friend. John Lloyd built the CPC measurement set-up and so much else. You were a dependable, resourceful colleague and provided an example I aspire to. Cris Flowers was my sounding board for everything from lab safety to optical measurements to office etiquette. Thank you for listening, for your thoughtful responses, and for asking me when you had questions too. Pilar Espinet, Annabelle Sibue, Michelle Dee, and Dirk-Jan Spaandermann made a variety of contributions to our sprawling project including cell measurements, CPC fabrication, CPC procurement and mechanical design. Rebekah Feist, Weijun Zhou and Jim Stevens from Dow provided support, encouragement and guidance.

For the TLSC project, Noah Bronstein from Berkeley introduced us to the Monte Carlo model that he and Vivian Ferry developed for LSC. David Needell took up that the modeling mantle. Colton Bukowsky designed the DBR filters.

The Atwater group has many resources and facilities primarily maintained by fellow group members. Nick Batara trained me on and maintained both the ellipsometer and the group computers for most of my graduate career. I am deeply indebted, as both were primary tools. Davis Darvish got me started on the group computer cluster and Phil Jahelka has been fielding my tech questions most recently. Lab safety officers Jeff Bosco, Rebecca Glaudell, Kelly Mauser and Cris Flowers trained, consulted and guided the rest of us. Ragip Pala set up and trained me on the SARP system; Giulia and Siying provided additional help. Jing-Shun Huang maintained the sputterer with me. Emily Warmann, Hal Emmer and Siying Peng all helped me with the confocal microscope. Hal Emmer taught me a little bit about vacuum systems and a lot about common-sense trouble-shooting of equipment. Dagny Fleischman trained me on the ebeam evaporator. Rebecca Saive trained me on the AFM. Ray Weitekampe and Adam Pietrick trained me help with the MMRC integrating sphere. I used Ali Ghaffari's PDMS lab extensively, and he deserves thanks for increasing order in our sometimes chaotic labs.

In addition, all the members and affiliates of the Atwater group I overlapped with. You contributed to my work and had on-going impacts on how I think about my work. You listened to my group meeting presentations and practice talks for conferences, asked questions, discussed your own work, and answered my random questions about software, tools, physics and managing up. There are too many people to name and I will surely forget too many, so thank you all.

All the administrative support I received from Christy Jenstad, Tiffany Kimoto, Jennifer Blankenship, Liz Jennings, Lyann Lau, Connie Rodriguez, Michelle Rodriguez, Tess Legaspi, Natalie Gilmore, Mary Sikora and Helen Duong over the years made the ride smoother and more pleasant. In the KNI I received training and help from staff members Melissa Melendes, Guy de Rose, Matt Sullivan Hunt, Nils Asplund, and Steven Martinez. The collaborative environment of KNI relies on a collaborative user environment. Thanks to Max Jones, Yu Horie, and Amir Arbabi for guidance on fabrication work.

Finally, I must acknowledge my master's advisor Pascale Chenevier. Working in her lab prompted my interest in continuing my scientific education by pursuing a Ph.D. My friends Jackie and Sarah convinced me to apply to Caltech. Once I got here, my entering first year materials science class and the many others we adopted into the lunch table crew including Andrew Hoff, Max Murialdo, Renee McVay, Mark Harfouche, Kevin Fiedler, Ivan Papusha, provided both social respite from work and

added breadth to my Caltech education. To my friends Sam, Erik, Jackie, Sarah, Chengyun, Lisa - thank you! There is too much to say to say more than that. Finally, my parents and Oliver pushed and reminded me that good enough and finished is the goal, even when I did not receive that advice gracefully or gratefully.

ABSTRACT

While the price of solar energy has dropped dramatically in the last few years, costs must be further reduced to reach wide-scale adoption. One strategy to decrease cost is to increase efficiency. Photovoltaic energy conversion is most efficient for a narrow frequency range. Lack of absorption of low energy photons and thermalization of high-energy photons leads lead to a loss of over 40% of incident solar power on a silicon cell. Current-matching and lattice-matching restrictions limit the efficiency of traditional monolithic multijunction solar cells. In order to avoid these limitations and realize ultrahigh efficiency (close to 50%), this thesis explores use of optical elements to split broadband sunlight into multiple spectral bands that can each be sent to physically separated solar cells tuned to best convert that band.

Design of a holographic diffraction grating based spectrum-splitting system resulted in a simulated module efficiency of 37%, meeting the efficiency of state-of-the-art modules. One of four holographic grating stacks is experimentally characterized. Next, a design incorporating dichroic filters, seven subcells with bandgaps spanning the solar spectrum, and concentrators with efficiency potential exceeding 45% module efficiency is presented. While prototyping this design, we also used on-going cost-modeling to ensure that our design was on-track to be a high-volume technology with low lifetime energy cost.

Finally, high-contrast gratings are used as resonant, dielectric spectrally selective mirrors in a tandem luminescent solar concentrator and as alternatives to Bragg reflectors. Gratings can have omnidirectional, high reflectivity by appropriately offsetting grating resonances in nano-patterned subwavelength thickness high-refractive index material. Subwavelength feature sizes suppress diffraction, and the high-refractive index of the grating layer leads to relatively angle-insensitive reflectance. Gratings can be fabricated by nanoimprint lithography, making them a scalable and economical option for photovoltaic applications. Simulations show hemispherically average reflectivity near 90% possible from a single subwavelength thickness layer. These properties are well suited for a variety of applications including multiple spectrum-splitting device architectures.

PUBLISHED CONTENT AND CONTRIBUTIONS

[1] M. D. Escarra, S. Darbe, E. C. Warmann, and H. A. Atwater, "Spectral-splitting photovoltaics: Holographic spectrum splitting in eight-junction, ultra-high efficiency module," in *IEEE PVSC 39*, 2013. DOI: http://dx.doi.org/10.1109/PVSC.2013.6744503,
S.D. participated in the conception of the project and performed holographic grating simulations.

[2] S. Darbe, M. D. Escarra, E. C. Warmann, and H. A. Atwater, "Spectral-splitting photovoltaics: Holographic spectrum splitting in eight-junction, ultra-high efficiency module," in *High and Low Concentrator Systems for Solar Electric Applications VIII*, 2013. DOI: http://dx.doi.org/10.1117/12.2024610,
S.D. participated in the conception of the project, performed holographic grating simulations, and wrote the manuscript.

[3] S. Darbe and H. A. Atwater, "Resonant dielectric high-contrast gratings as spectrum splitting optical elements for ultrahigh efficiency (>50%) photovoltaics," in *IEEE PVSC 42*, 2015. DOI: http://dx.doi.org/10.1109/PVSC.2015.7356160,
S.D. performed optical simulations, data analysis, and wrote the manuscript.

[4] C. N. Eisler, C. A. Flowers, P. Espinet, S. Darbe, E. C. Warmann, J. Lloyd, M. Dee, and H. A. Atwater, "Designing and prototyping the polyhedral specular reflector, a spectrum-splitting module with projected >50% efficiency," in *IEEE PVSC 42*, 2015. DOI: http://dx.doi.org/10.1109/PVSC.2015.7356406,
S.D. participated in spectrum-splitting optical element prototype and concentrator fabrication.

TABLE OF CONTENTS

LIST OF ILLUSTRATIONS

LIST OF TABLES

NOMENCLATURE

$\$/W_p$. Cost per peak power rating of a photovoltaic system. E.g. If a silicon module costs $200 and has a maximum power of 200 W, its $\$/W_p$ cost is $\$1/W_p$.

μ. Electrochemical potential.

azimuthal angle. Longitude angle.

B270. A common variety of glass.

bankability. Ability to obtain financing..

BFO. Bismuth ferrite.

BOS. Balance of System - all non-module costs of an installed photovoltaic system.

bypass diode. In strings of solar cells if any one unit fails, the whole unit's energy production can be lost as the failed unit starts acting as a resistor. A bypass diode is triggered by such a situation to put such cells either shadowed during part of the day or damaged into open circuit to prevent this.

chirp. To modify the period of a grating as a function of position in one or more spatial dimension such that the final structure is quasi-periodic structure.

CNC. Computer numerical control, as in CNC machine tools, which are automated rather than manually controlled.

CPC. Compound parabolic concentrator.

CPV. Concentrating photovoltaics.

DBR. Distributed Bragg reflector.

DCG. Dichromated gelatin.

DNI. Direct normal incidence, includes both light directly from the sun and circumsolar irradiance, which is the halo around the sun caused by atmospheric scattering.

ebeam. Electron beam.

EQE. External quantum efficiency.

ERE. External radiative efficiency.

escape cone. The cone of angles not trapped by total internal reflection in a higher refractive index material at its interface with a lower refractive index material defined by the critical angle given by Snell's law.

HCG. High-contrast grating.

HCPV. High concentration photovoltaics.

HIT cell. Silicon Heterojunction with Intrinsic Thin layer solar cell device design.

HOE. Holographic optical element.

HSS. Holographic spectrum splitter.

IQE. Internal quantum efficiency.

IRE. Internal radiative efficiency.

k. Boltzmann constant.

LCOE. Levelized cost of electricity.

LSC. Luminescent solar concentrator.

module. Discrete power producing unit of a photovoltaic system. In CPV, modules are sometimes grouped to be installed on a single tracker.

negative resist. Polymerizes where exposed.

NPV. Net present value.

NREL. National Renewable Energy Laboratory.

packing fraction. In photovoltaics, this is the land area covered by solar collectors when the sun is straight ahead.

PDMS. Polydimethyl siloxane.

polar angle. Angle measured from the grating normal, latitude angle.

positive resist. Dissolves where exposed.

PSR. Polyhedral Specular Reflector.

PV. Photovoltaic.

RCWA. Rigorous coupled wave analysis.

rms. Root mean squared.

runner. The pathway for plastic in an injection mold between the auger where it is melted and the mold cavity. The runners have pinch points at the interface with the part from which they can be easily separated. This process leaves a small nub..

TIR. Total internal reflection.

TMCS. Trimethylchlorosilane.

UV. Ultraviolet.

VPH. Volume phase hologram.

Chapter 1

INTRODUCTION

1.1 Motivation for photovoltaics

Solar energy is a clean, abundantly available power source. As threats of climate change grow more urgent, a carbon neutral power supply is critical. Solar energy is additionally a distributed resource, which makes it a useful power source in areas without reliable grid connection, such as in developing countries or war zones. A variety of factors prevent wide-scale adoption of PV. The cost is nearing and in some cases has hit levels that have been cited as targets for 'grid parity'. However, solar energy is not a dispatchable energy source. This creates some natural limits for how much of the power generation mix can come from solar. Older, inadequate grid technology also prevents effective transportation of power across the United States to balance supply and demand. The more favorable cost metrics can be, the more pressure there will be to innovate and tackle these other challenges head-on. In the past few years, the cost of silicon modules has plummeted. In fact, goals set by the Department of Energy Sunshot program of <$/W module cost and <$0.06/kWh for 2020 have been met early. However, remaining system costs, referred to as Balance of System costs, including mounting and electrical hardware, permitting, and installation have not gone down as fast. Increasing the efficiency of a solar module better leverages these fixed costs, decreasing overall solar energy cost.

1.2 Spectrum-splitting photovoltaics

Single-junction photovoltaics have a theoretical detailed-balance efficiency limit of about 33%. [1] A great deal of research and development have led to crystalline silicon and GaAs cells which approach this thermodynamic limit with record efficiencies of 25.6% and 28.8%, respectively. [2] To increase photovoltaic conversion efficiency beyond this, we turn to multijunction solar cells, which address losses due to lack of absorption of photons with energy below the solar cell material bandgap energy and also address losses due to thermalization of carriers generated by photons with energy greater than the bandgap energy. Together these two losses add up to over 40% of total incident solar power. [3] The higher bandgap cells must generate a higher collection voltage for the spectrum splitting to be worthwhile. For high-quality semiconductor materials the V_{OC} of the solar cell is almost linearly related to

the bandgap of the semiconductor material. [4] Thus using higher bandgap materials to collect higher energy photons returns more electrical energy upon absorption and collection. This motivates incorporation of many, high quality absorber materials into a photovoltaic conversion system. The III-V compound semiconductor system provides direct bandgap materials of high material quality with bandgap tunability over much of the target range of interest for solar applications, so we focus on this material system.

Many methods have been explored for incorporating multiple absorbers into photovoltaic devices. In the past decade, epitaxially grown, monolithic tandem cells (typically 2-4 absorbers) have been the focus of research and development. This kind of cell has the advantage of intrinsic splitting of the solar spectrum into different frequency bands. Each cell acts as a long-pass filter allowing lower energy, unabsorbed photons to pass through to the next cell. However, this device architecture has a series of limitations. First of all, high-quality material requires low defect density in the single crystal material. One way to accomplish this is for all layers to be lattice-matched, which restricts choice in the bandgap of each subcell. Alternatively, incorporating subcells which are not lattice matched imposes a requirement for metamorphic buffer layers [5] which adds complexity. Secondly, since monolithic tandem cells are electrically in series, each junction is limited by the current generated by the cell in the stack which generates the least current. These cells are designed so that this current-matching condition maximizes current for a particular solar spectrum. As the solar input varies over the course of a day or year or with changing location, the current match may no longer hold, decreasing efficiency. Finally, for each additional subcell a tunnel junction must also be designed which allows the series electrical connection between each pair of subcells. These three factors limit the number of subcells one can incorporate into monolithic tandem cells. These factors lead to low marginal return on incorporating additional subcells. [6] In a spectrum-splitting architecture, optics external to the cells separate solar light into bands which are directed to an appropriate receiver made up of a cell of tuned bandgap and possibly a concentrating optic. By incorporating many high quality, independently connected subcells of different bandgaps along with high concentration, this approach could lead to higher efficiencies than have been demonstrated by today's monolithic multijunction devices. This spectral-splitting optic also allows each cell to act electrically independently, enhancing annual energy production. [6]

DARPA's Very High Efficiency Solar Cells program set a goal of 50% cell efficiency and funded the current spectrum splitting efficiency record holder which incorporated two multijunction solar cells for a total of five subcells giving 38.5% submodule efficiency. [7] Their spectrum splitting optical element was a Bragg reflector. A full module made with this design was demonstrated to have 36.7% efficiency. [8] The current module efficiency record of 38.9% is held by a four-junction tandem concentrating photovoltaic module. [9] Other recent efforts have used diffraction [10], refraction [11], specular reflection [12], and diffuse reflection [13] to split the solar spectrum. Imenes and Mills [14] reviewed spectrum splitting technologies in 2004 and in 2013 Mojiri et al. provided an update. [15] and also provided a more recent update to their original review. Groups have also worked on holographic approaches. [16],[17] The efficiencies of lateral multijunction devices, however, still lag behind those of traditional multijunction cells and devices.

1.3 Full Spectrum Photovoltaics Project

The Caltech Full Spectrum Photovoltaics Project sought to take advantage of the efficiency benefits of spectrum-splitting to make a 50% module efficiency photovoltaic system. We begin with an internal design competition among three designs. The Polyhedral Specular Reflector (PSR), Holographic Spectrum Splitter (HSS) and the Light Trapping Filtered Concentrator (LTFC). I discuss the HSS in Chapter 2. Work on the LTFC was undertaken by Emily Kosten and John Lloyd. Both the HSS and LTFC had lower optimized simulated efficiency than the Polyhedral Specular Reflector so the latter was chosen as the winner of our internal design competition. We made four functioning optoelectronic submodule prototypes of the PSR as well as intermediate partial prototypes. Ongoing prototyping efforts are underway at the time of this writing. Chapter 3 gives a brief review of design generations and prototype fabrication and performance of the PSR. In more detail, Chapter 4 discusses production of concentrators for prototyping. Chapter 5 explores commercial prospects of the technology. Finally, Chapter 6 covers work on high-contrast grating filters. These near-subwavelength scale optical elements display relatively angle-independent reflectivity with a single subwavelength thickness layer of high refractive index material. This makes them promising in a number of applications, including a variety of spectrum-splitting architectures. In this thesis, they are explored by simulation as an alternative to Bragg mirrors in the PSR as well as for a tandem luminescent solar concentrator.

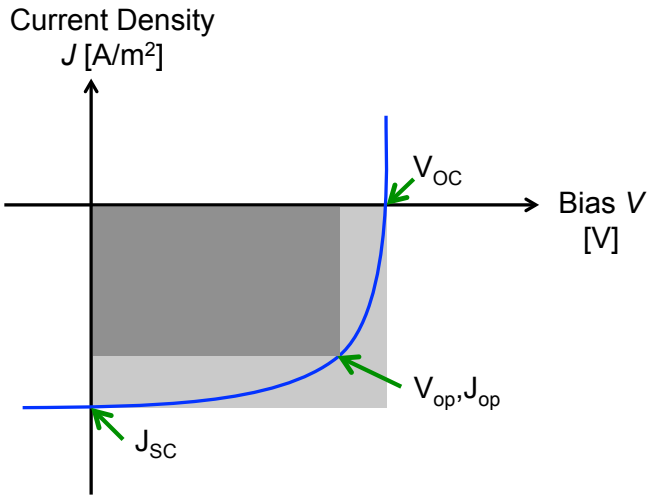

Figure 1.1: Example of a J-V Curve.

1.4 Photovoltaic energy conversation

Photovoltaics are devices that collect the energy imparted to a material by incident light promoting an electron from lower energy state to a higher energy state. Generally speaking this is done in a semiconductor material with the electron promoted from the valence band (the highest energy occupied band) to the conduction band (the lowest energy unoccupied band), leaving an electron vacancy or 'hole'. Rather than decaying back to the ground state by emitting a photon (radiative recombination) or losing energy as heat to the atoms in the material (non-radiative recombination), the excited electron can be collected and run through an external circuit to do useful work. The power P collected by a solar cell is equal to

$$P = V_{op} \times J_{op} = V_{OC} \times J_{SC} \times FF, \tag{1.1}$$

where V_{op} is the voltage and J_{op} the current density produced by the cell when operating at its maximum power point, V_{OC} the voltage of the device at open circuit, J_{SC} is the current that flows in the device at zero bias, and the fill fraction FF the ratio of $V_{op} \times J_{op}$ and $V_{OC} \times J_{SC}$. Fill fraction is a metric for the squareness of the J-V curve, or in other words, of how close the operating performance reaches the potential of that device, as illustrated in Figure 1.1.

The current in the solar cell is determined by how many above-bandgap energy, incident photon are absorbed in the material and collected. The voltage is determined by the quasi-Fermi level separation of electrons and holes in the material. The Fermi energy is the energy level at which the probability of electron occupation is 1/2. At absolute zero, the probably of electron occupation of ground states is 1 while the

probability of occupation of excited states is zero, and the Fermi level lies half-way between the highest energy occupied state and the lowest energy unoccupied state in an undoped semiconductor. At finite temperatures, the probability of occupation changes more gradually from high to low, but as long as the material is at equilibrium the Fermi energy stays the same. When an external energy source is introduced, such as solar illumination, the electrochemical potential of electrons in the material is no longer zero. The quasi-Fermi level splitting indicates the potential difference between excited electrons in the conduction band and excited holes in the valence band. As the charge carrier density goes up, the voltage of the cell goes up, increasing the efficiency of collection. Thus, solar cells illuminated by concentrated sunlight have higher efficiency.

In fact, any effects which increase the ratio of photogenerated current to dark current in the solar cell confer this voltage advantage. Thus if an equal number of photons can be captured by a thinner layer of semiconductor material, there is also a voltage advantage. This can be accomplished by thinning the cell and adding a metallic reflector to the back side. This always a cell to be half as thick as it otherwise would be. Such a back-reflector is added to the single-junction solar cells in our design, but including a sacrificial layer between the active cell layers and semiconductor growth substrate. This layer can be selectively etched away leaving a couple of micron thick free standing solar cell which can have a metallic back reflector deposited on it. Silicon solar cells must be much thicker than III-V solar cells as it absorbs weakly since it has an indirect bandgap. For silicon, rather than a back reflector, the front face of the cell is roughened, significantly increasing the path length of light in the cell (far beyond the factor of two imparted by a back-reflector). [18]

1.5 Relevant optical concepts

Some optical concepts are relevant to work presented in multiple chapters, so I will quickly summarize them here. Light at an interface refracts according to Snell's law,

$$n_1 \sin\theta_1 = n_2 \sin\theta_2 \tag{1.2}$$

where n_i is the refractive index of medium i and θ_i is the direction of propagation measured from the interface normal. Any time light passes through an interface between two materials with dissimilar refractive index there is some reflection given by the Fresnel equations,

$$R_s = \left| \frac{n_1 \cos\theta_1 - n_2 \cos\theta_2}{n_1 \cos\theta_1 + n_2 \cos\theta_2} \right|^2 \tag{1.3}$$

for s or transverse electric (TE) polarization, and

$$R_p = \left| \frac{n_1 \cos\theta_2 - n_2 \cos\theta_1}{n_1 \cos\theta_2 + n_2 \cos\theta_1} \right|^2 \tag{1.4}$$

for p or transverse magnetic (TM) polarization. The polarizations are defined relative to the plane defined by the direction of propagation of light and interface normal. The TE polarization has its electric field vector normal to this plane while for the TM polarization the electric field vector lies in this plane. The behavior of totally unpolarized light can be obtained by averaging the behavior of the two orthogonal polarizations. At Brewster's angle given by

$$\theta_B = arctan\left(\frac{n_2}{n_1}\right), \tag{1.5}$$

R_p goes to zero and the reflected light is only s-polarized. For non-scattering media, the conservation of energy requires $R + T + A = 1$ where R is reflection, T is transmission and A absorption. These reflections coupled with interference effects are exploited in the design of antireflection coatings. The reflectivity of an interface can be decreased using a single thin-film with refractive index $n = \sqrt{n_1 n_2}$ and thickness $\frac{\lambda_0}{4n}$ where λ_0 is the free-space wavelength, n is the refractive index of the antireflection layer and n_1 and n_2 are the refractive indices of the materials on either side of the interface. This occurs because the reflection off the first thin-film interface is of similar amplitude but completely out of phase with the reflection off the back interface causing destructive interference. In contrast, to design a Bragg reflector, one creates a series of interfaces from which the reflected waves constructively interfere. The weak resonances that occur within a thin film due to these interfacial reflections are called Fabry-Perot resonances.

Compound parabolic concentrator

A compound parabolic concentrator (CPC) or Winston cone (named for Roland Winston, who wrote the book [19] and the seminal paper [20] on CPC) is a type of concentrating optical element that is thermodynamically ideal. That is, nearly all light within a certain acceptance angle range θ_{in} is transmitted to the output face, and light outside that acceptance range of angles is not propagated as shows in the blue trace in Figure 1.3. It provides the maximum amount of concentration possible given the angular spread of incident light to be concentrated. It is only possible to concentrate light that has less than maximal directional entropy. In effect, concentrating light is trading off spatial entropy for angular entropy. You

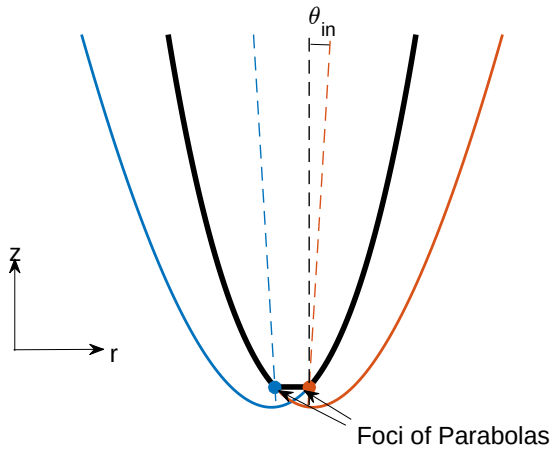

Figure 1.2: Construction of compound parabolic concentrator profile.

can concentrate perfectly collimated light to a diffraction limited spot but cannot concentrate the light of a Lambertian source at all. This principle, often called the brightness theorem or conservation of etendue, is the ultimate limit of the degree of concentration of an optical element,

$$C_{max} = \frac{n_{out} \sin \theta_{out}}{n_{in} \sin \theta_{in}}, \tag{1.6}$$

where C_{max} is the maximum degree of concentration, n_{out} the refractive index of the output medium, n_{in} the refractive index of the incident medium, θ_{out} the maximum angular spread of the concentrated light, and θ_{in} the maximum angular spread of the incident light. The degree of concentration C is the increase in optical power per unit area of the source relative to the output and is either or in the context of photovoltaics expressed as a number of 'Suns', e.g. silicon cells on SunPower's C7 concentrator receive 7 Suns. By pointing a concentrator directly at the sun and restricting θ_{in} to just the solid angle subtended by the sun itself, the maximum possible concentration is around 54,000X. More typically, in concentrating photovoltaics the maximum concentration used is around 1000X with an input angle of 1° to allow for errors in point accuracy of a solar tracker, displacements due to environmental factors such as wind, and to collect circumsolar irradiance (light that is mildly scattered by the atmosphere).

The profile of a CPC is given by

$$(r\cos\theta_{max} + z\sin\theta_{max})^2 + 2a'(1+\sin\theta_{max})^2 r - 2a'\cos\theta_{max}(2+\sin\theta_{max})^2 z - a'^2(1+\sin\theta_{max})(3+\sin\theta_{max}) = 0, \quad (1.7)$$

where 2a' is the width of the output aperture, θ_{max} is the acceptance angle of the CPC, and z is the concentrator height and is zero at the center of the output face, and at $z = 0$, with $r = 0$ as the centerline of the concentrator, $r = a'$. For a circular CPC, this profile is revolved ($r^2 = x^2 + y^2$). For a trough CPC, the profile is extruded in the directional orthogonal to the $r - z$ plane. A square or rectangular CPC is defined by the intersection of two orthogonal trough CPC. Revolved and extruded CPC profiles have fewer aberrations from ideal concentrator behavior than other shapes (see Figure 1.3). Circular cross-section CPC are also much easier to produce due to their rotational symmetry than square cross-section parts, but tiling circular primary CPC would only fill 90.6% of the module input leading to a large aperture area efficiency loss. One arrives at this equation for the profile in the following way: take two identical parabolas with their foci horizontally offset from one another by $2a'$, and tilt each away from the other by angle θ_{max} from the vertical axis. The left side of the parabola on the right and the right side of the parabola on the left, the inside legs, define the CPC curvature as illustrated in Figure 1.2. The straight line between the two foci is the output face. Selecting an acceptance angle and an output area determines the input area and thus the height of the structure as well assuming maximal output angular spread of $\theta_{out} = 90°$. However, for practical photovoltaic systems, the concentrator-cell interface will experience too much Fresnel reflection to have a full hemispherical range of output angles. By adding a conic section at the bottom of the ideal CPC, output angular spread can be decreased at the expense of slightly increased height.

As suggested by Equation 1.7, the medium of the CPC can be air or some other material. If the medium is air, the profile is made by reflective sides, for example, curved silver mirrors. Alternatively, with a solid dielectric material, the reflection comes from total internal reflection (TIR) due to grazing incident angles. As long as the surface quality is high, the reflectivity of total internal reflection is higher than the reflectivity of an air-metal interface with experiences some absorption. There is also a boost in the degree of concentration by a factor of n_{CPC} for a trough concentrator or of n_{CPC}^2 for a square or circular CPC. The downsides of the solid optic include greater weight and volume of material for a comparable size CPC

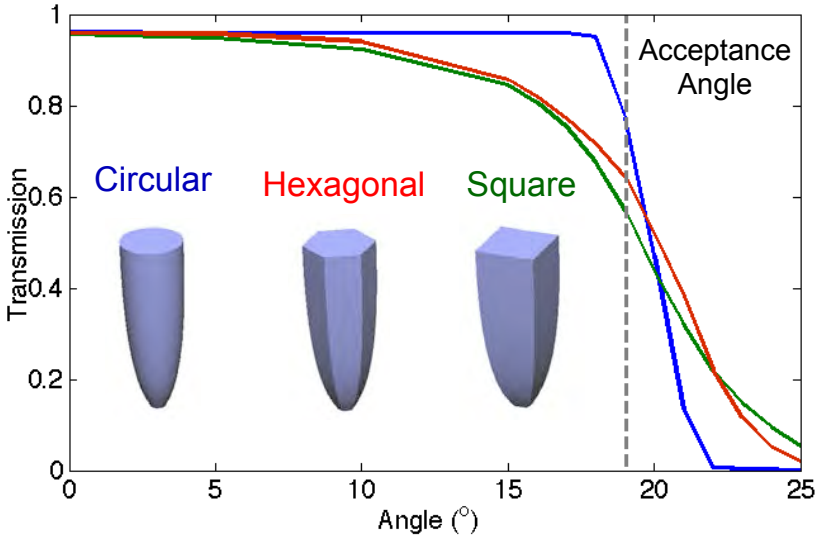

Figure 1.3: Transmission efficiency as a function of incident angle for circular (blue), hexagonal (red) and square (green) cross-section compound parabolic concentrators.

and greater need for high surface quality and cleanliness to ensure that light is not scattered out but successfully reflected by TIR and retained in the concentrator.

While the full height of the gives the highest efficiency of transmission from input to output face for the whole acceptance angle range, truncating a CPC from the top even down to a significant fraction of its intended height decreases efficiency in a nonlinear way. Even down to half the intended profile, much of the intended concentration is retained. Ray tracing simulations of CPC for the Holographic Spectrum Splitter design in Section 2.3 explore the efficiency drop-off. CPC fabrication is described in Chapter 4.